

Observation of long-term changes in the effective refractive index of light

A. C. Melissinos

*Department of Physics and Astronomy, University of Rochester
Rochester, NY 14627-0171, USA*

14 January 2019

1 Tidal gravity gradients

During the LIGO S5 Science run (April 2006 to June 2007) preliminary data from the H1 interferometer (Hanford site) recorded long-term changes in the effective refractive index of light over a 14 month period [1]. By changes in the effective refractive index, $d\bar{n}/\bar{n}$ we imply variations in the phase velocity, or equivalently the frequency of the light due to external factors such as gravitational gradients. Time dependent gravitational gradients are present along the arms of the interferometer because of the horizontal component of the tidal forces, which is typically of order $g_{hor} \approx 10^{-7}g \approx 10^{-6} \text{ m/s}^2$ [2].

Changes in $d\bar{n}/\bar{n}$ are recorded by the DARM-CTRL channel of the interferometer, which is also available in minute trends. DARM-CTRL is the output of an integrator fed by the error signal, DARM-ERR, proportional to the intensity of the light reaching the antisymmetric (dark) port, ASQ¹. It is proportional to the difference in phase shift of the light returning from the two arms

$$\Delta\phi = \delta\phi_1 - \delta\phi_2. \quad (1)$$

The phase shift $\delta\phi_j$ in each arm is,

$$\frac{\delta\phi_j}{2\pi} = \left(\frac{\delta L_j}{L} + \frac{\delta f_j}{f_0} + \frac{\delta \bar{n}_j}{\bar{n}} \right) \frac{2L}{\lambda}, \quad (2)$$

and depends on the arm length L_j , the frequency of the (carrier) light f_0 , and the effective refractive index, \bar{n}_j ; λ is the wavelength of the carrier.

When the interferometer is “locked” onto a dark fringe, $\Delta\phi = 0$, and this is achieved by adjusting both the (microscopic) arm length difference, $\delta L = L_1 - L_2 = 0$ (modulo λ), as well as the frequency of the carrier, δf_0 . However, $\delta \bar{n}$ is determined by external factors and *can not be adjusted*. Departures from $\Delta\phi = 0$ are recorded with high bandwidth (at 16.384 kHz) and this “error signal” is the output of the instrument. Similarly, the corrective actions of the servo mechanisms, that return $\Delta\phi \rightarrow 0$ are recorded and are available for analysis.

Integration of the error signal over a sufficiently long time interval T , as compared to the servo response, yields

$$\frac{1}{T} \int_{t-T/2}^{t+T/2} \frac{\Delta\phi}{2\pi} dt \rightarrow \frac{1}{T} \frac{2L}{\lambda} \int_{t-T/2}^{t+T/2} \frac{\Delta\bar{n}}{\bar{n}} dt = \frac{2L}{\lambda} \left\langle \frac{\Delta\bar{n}}{\bar{n}} \right\rangle \quad (3)$$

¹Abbreviations: DARM Differential Arm Control, ASQ Antisymmetric Port, Quadrature phase.

because when the interferometer is locked, the first two terms in Eq.(2) have been returned to zero by the servo, while their fluctuations are stochastic and average to zero. This shows that the interferometer is sensitive to time-varying signals from Lorentz violation in the effective refractive index \bar{n} . Returning to Eq(2) we see that after the action of the servo,

$$\delta L = \delta L_1 - \delta L_2 = 0$$

while $\delta f = 0$ by the configuration of the interferometer, but $\delta\bar{n}$ has not been changed. Therefore the DARM-CTRL signal at time t , which is given by Eq.(3), is a direct measure of $\delta\bar{n}(t)/\bar{n}$.

To estimate the observable signal we recall that the horizontal component of the tidal forces along the arms, $g_{hor} \approx 10^{-7}g \approx 10^{-6} \text{ m/s}^2$, is time-dependent and modulated at distinct frequencies at the daily and twice daily region [2].

In the weak field approximation, the presence of a gravitational potential Φ modifies the g_{00} metric coefficient

$$g_{00} = -(1 - 2\Phi/c^2) \quad (4)$$

The departure of g_{00} from its flat space value gives rise to time dilation, or equivalently to a shift in the frequency of light propagating through that gravitational field [3, 4].

$$\nu_A - \nu_B = -\frac{\Phi_A - \Phi_B}{c^2} \nu \quad \text{or} \quad \frac{\delta\nu}{\nu} = \frac{\delta\bar{n}}{\bar{n}} = -\frac{\delta\Phi}{c^2}, \quad (5)$$

with $\bar{n} = c'/c$ the effective refractive index, which is often used in the literature to indicate frequency shifts.

A constant gradient g_{hor} along the x -direction can be described by a potential, $\Phi(x) = -g_{hor}x$. Thus light executing a single round trip in an arm of length L acquires a phase shift (as compared to light traveling in a field-free region) equal to

$$\delta\phi^{(s)} = 2 \int_0^L \delta\omega dt = 4\pi\nu_0 \int_0^L \frac{\delta\nu}{\nu} \frac{dx}{c} = -\frac{4\pi}{\lambda_0} \int_0^L \frac{\Phi(x)}{c^2} dx = \frac{2\pi}{\lambda_0} \frac{g_{hor}L^2}{c^2}. \quad (6)$$

Numerically, for $g_{hor} = 10^{-6} \text{ m/s}^2$ and for a single traversal in the arms

$$\frac{\Delta\phi^{(s)}}{2\pi} \approx 2 \times 10^{-10}.$$

This is the same phase shift as generated (in a single traversal) by a strain $h = 2.5 \times 10^{-20}$ imposed on the interferometer.

This effect represents the *direct coupling* of the tidal gravitational gradient to the light circulating in the interferometer and is present while the interferometer remains locked. The phase shift induced by the tidal gradients can be seen in Fig.(1) where DARM-CTRL is plotted for 21 days of the S-5 data. Note that when lock is lost DARM-CTRL is reset to zero.

2 Readout at the fsr frequency

The measurement of $d\bar{n}/\bar{n}$ can be extended to a continuous time record (as compared to only lock segments) by taking advantage of the signal at the FSR (Free Spectral Range) frequency, which was operational during the S5 run. The implementation and properties of the FSR channel are summarized in the Appendix. As discussed there, the FSR channel offers advantages for the detection of low frequency signals, well below 40 Hz, the typical cut-off in the conventional detection band. It is particularly well suited for the detection of very low frequency signals such as induced by the tidal gradients or equivalently due to long term changes in effective refractive index.

The *calibrated* strain sensitivity in the FSR region, 37.504 ± 1 kHz, averaged over the entire S5 run is shown in Fig.(2). There is no seismic wall, while the discrete lines are due to mechanical resonances in the test masses (the mirrors) in the arms. The data in the region $f = f_{fsr} \pm (1 \text{ kHz})$, are decimated to 16.384 kHz and written to 64 s long frames. We Fourier transform 8 second long segments of data, and average eight such segments to obtain a power spectrum for every (64 second long) frame. We then integrate the spectral power density in the frequency range $f = f_{fsr} \pm (200 \text{ Hz})$, including an appropriate filter². The integrated power, evaluated every 64 seconds, represents a time series of the slowly changing difference in phase shift between the interferometer arms. This series is shown in Fig.(3) for the H1 interferometer for the entire 14 month long S5 run, April 2006 to July 2007. Daily and twice-daily modulation is evident by inspection as is an unexpected strong modulation with period of half a year.

Choosing the central part of the fsr spectrum implies that the data presented in Fig.(3) are sensitive only to very low modulation frequencies, a condition also imposed by the long integration time of 64 s. The time series shown in Fig.(3) is not affected by the repeated loss of lock during the long run, that affects the DARM-CTRL signal seen in Fig.(1), because it is referenced to the biasing phase shift that remains constant, see Eq.(15); compare to Fig.(1). This is further confirmed by an expanded plot of the data where the fsr signal is seen to “recover” after a loss of lock [5].

To examine the cause of the observed modulation we Fourier analyze the 14-month long time series [6] shown in Fig.(3). Since the data are not continuous an FFT is not applicable, but instead we use the Lomb-Scargle algorithm [7] which fits the data to a sine and a cosine series. The spectra (of the integrated power at the fsr) are shown in Fig.(4) for the region of daily frequencies and in Fig.(5) for the region of twice-daily frequencies. The measured frequencies are listed in Table 1, where they are also compared with the known values [2].

The agreement between the measured and known frequencies of the tidal lines is excellent within the resolution of the measurement which is³ $\Delta\nu_{res} = 1/(4T_{total}) = 6 \times 10^{-9}$ Hz, with $T_{total} = 4.2 \times 10^7$ seconds. Comparing the observed frequencies to the predicted ones,

²Proportional to the arm cavity resonance, to emphasize the region in the vicinity of the fsr frequency, i.e. at very low modulation frequencies

³The factor of 4 is included because in the spectral analysis [7] the data was oversampled by a factor of four.

and using $\Delta\nu_{res}$ as the measurement error, yields $\chi^2/DF = 1.86$. The Table also lists the observed long-term, twice yearly, component.

Table I. Observed and known frequencies of the tidal components (Hz)

Symbol	Measured	Predicted	Origin, L=lunar; S=solar
<u>Long period</u>			
S _{s_a}	6.239×10^{-8}	6.338×10^{-8}	S declinational
<u>Diurnal</u>			
O ₁	1.07601×10^{-5}	1.07585×10^{-5}	L principal lunar wave
P ₁	1.15384×10^{-5}	1.15424×10^{-5}	S solar principal wave
S ₁	1.15741×10^{-5}	1.15741×10^{-5}	S elliptic wave of ^s K ₁
^m K ₁ , ^s K ₁	1.16216×10^{-5}	1.16058×10^{-5}	L,S declinational waves
<u>Twice-daily</u>			
N ₂	2.19240×10^{-5}	2.19442×10^{-5}	L major elliptic wave of M ₂
M ₂	2.23639×10^{-5}	2.23643×10^{-5}	L principal wave
S ₂	2.31482×10^{-5}	2.31481×10^{-5}	S principal wave
^m K ₂ , ^s K ₂	2.31957×10^{-5}	2.32115×10^{-5}	L,S declinational waves

The presence of the Earth tides is well known and must be compensated in order to keep the interferometer in lock. The observed signal, that is, the phase shift in the light returning from the two arms, is not due to a change in the arm lengths, after all the interferometer is locked, but to the change in the effective refractive index of the light traveling in the arms. As already discussed, the change in refractive index, or equivalently in frequency, is caused by the horizontal component of the tidal acceleration along the arms which is modulated at the tidal frequencies.

3 A modern Michelson-Morley experiment

As an application of readout at the fsr frequency we discuss the limits on changes in the refractive index of light as a function of the orientation of the interferometer arms due to the motion of the Earth with respect to an absolute reference frame (Lorentz Invariance) [8, 1], as obtained using the preliminary LIGO data from the S5 run [6]. The interferometer is kept on a dark fringe and the observable signal is given by Eqs.(1-3).

The Earth's sidereal rotation frequency is $f_s = 1.16058 \times 10^{-5}$ Hz, while the frequency of the earth's annual rotation around the sun $f_a = 3.16876 \times 10^{-8}$ Hz. Such frequencies are outside the band of interest for gravitational wave searches, but can be accessed by down-sampling the signals in the DARM-CTRL channel, which, as already mentioned is an integral over the error signal. However it is preferable to examine the response of the fsr

channel, which is well adapted for the detection of very slowly varying signals, as discussed in the Appendix.

The spectrum of daily frequencies, shown in Fig.(4), contains a very strong line (S1) at the sidereal frequency (see Table I), far in excess of the expected tidal gradient and of disproportionately large amplitude when compared to the other lines in this and in the twice-daily frequency region. Therefore we attribute this line to human activity on a daily cycle and will not use the daily frequencies to examine refractive index variations. In contrast the lines at the twice daily frequencies N2, M2, S2 and K2, shown in Fig.(5), conform with the known tidal amplitudes. Before making a comparison of the data with the known tidal amplitudes we must calculate the horizontal component of the tidal force along the arms of the interferometer at the latitude of the Hanford site, and for the orientation of the two arms. For the dominant M2 line we find

$$F_{South} \approx 0.7 \times 10^{-6} \text{ m/s}^2 \qquad F_{West} \approx 10^{-6} \text{ m/s}^2$$

Thus the phase shift induced by the M2 line for a single traversal is

$$\Delta\phi^{(s)}/2\pi = 1.2 \times 10^{-10}$$

The measured power in the M2 line is obtained by integrating the spectral line in Fig.(5) over frequency⁴ and similarly for the K2 line which is at the twice daily sidereal frequency

M2	Measured power 3538 counts	Known amplitude 91 μGal
K2	Measured power 415 counts	Known amplitude 11.5 μGal

The expected tidal power in the K2 line (corresponding to 11.5 μGal) is 447 counts. Thus the observed non-tidal power at the twice sidereal frequency is

$$\text{K2}_{\text{non-tidal}} = 32 \pm 34 \text{ counts}$$

or

$$\delta\phi^{(s)}/2\pi = (1.1 \pm 1.2) \times 10^{-12} \quad \text{non-tidal}$$

It follows from Eqs(2,3) that the upper limit on Lorentz Invariance violation as deduced from (the absence) of change in the effective refractive index of light at the twice sidereal rotation frequency of the Earth, after accounting for the tidal gradients, is

$$\frac{\delta\bar{n}}{\bar{n}} \leq \frac{\delta\phi^{(s)}}{2\pi} \frac{\lambda}{2L} = (1.4 \pm 1.5) \times 10^{-22} \qquad (7)$$

This result is an improvement of four orders of magnitude over the existing limits on the effective refractive index of light [9], and it is compared in Fig.(6) to the results obtained, using interferometers and rotating cavities, over the past 140 years. The limits on the SME

⁴Since the true line width is narrower than the experimental resolution, the power is given by the area under the peak.

coefficients in the photon sector, as deduced from the above result, were given in [1] and are included in the most recent compilation from different experiments [11].

The measurement of the M2 tidal line can serve as a direct calibration of the power in the low frequency spectral lines in terms of the phase shift sensed by the interferometer at these frequencies. As discussed in the Appendix the expected phase shift at the M2 line reproduces the observed modulation of the fsr data. The power in the spectral lines was scaled by the *amplitude* of the tidal forces since the power in the tidal lines arises from the interference of the tidally induced phase shift with the biasing phase shift see Eq.(15).

4 The twice annual modulation

The twice annual modulation shown in Fig.(3), poses a problem. The low frequency part of the spectrum is plotted in Fig.(7) where the observed frequency $f = (6.239 \pm 0.6) \times 10^{-8}$ Hz agrees with twice the Earth's orbital frequency $f_{2\Omega} = 6.338 \times 10^{-8}$ Hz. In principle the observed twice annual modulation is a direct violation of Lorentz invariance. However when examined in the context of the pure-photon sector of the Standard Model Extension (SME) [10] this result is incompatible with the complete absence, in the same data set, of modulation at the yearly orbital frequency of the Earth, Ω . While it might be possible to explain this discrepancy by inclusion of other sectors of the SME, or by a phenomenological model, only a repeat of the above measurements can provide a definitive answer.

In view of this inconsistency we consider possible experimental causes for the clearly observed twice annual modulation seen in Fig.(3). It is evident that the major modulation, $M \approx 0.3$ is at exactly the twice yearly frequency, and one wonders how this frequency has been introduced into the data. There is a tidal component at this frequency, the solar declinational or "zonal" wave, S_{sa} . At the Hanford latitude, the vertical component of this wave has amplitude $A(S_{sa}) = 1.5 \mu\text{Gal}$, while the amplitude of the vertical component of the dominant M2 wave has amplitude $A(M2) = 43 \mu\text{Gal}$. The latter gives rise to modulation $M \approx 0.1$. Thus the observed twice annual modulation $M \approx 0.3$, can not be due to the "direct coupling" of the zonal tidal amplitude to the light in the interferometer.

A second possibility is that the zonal amplitude distorts the ground and introduces a time dependent *macroscopic* arm length difference which, of course, is not reset by the fast feedback that maintains the interferometer in lock. The zonal component introduces a strain of 2×10^{-9} [12], or a change in the arm length difference of $\delta\Delta L = 8 \times 10^{-6}$ m. In principle this is compensated by the tidal servo. If we assume that the arm extension due to the zonal wave remains uncompensated, leading to a change in the macroscopic arm difference, the maximal variation in the signal modulation is

$$\frac{\delta M}{M} = -\frac{\delta(\Delta L)}{\Delta L} \approx -4 \times 10^{-4}$$

as compared to the observed modulations

$$\text{Daily and Twice - Daily} \quad M \approx 0.1 \quad \text{and} \quad \text{Twice - Annual} \quad M \approx 0.3$$

A third possibility is that the tidal correction servo introduces a macroscopic arm length difference at the twice daily frequency. We examined the recorded tidal correction signal for the entire run. The correction for the daily and twice daily displacements is clearly present, and follows the tidal frequencies. However there is no indication in the spectrum of any significant modulation at the twice yearly, or yearly frequency.

While the daily and twice daily tidal signals are observed in the DARM-CTRL channel, the twice-annual modulation is absent. This can be understood because DARM-CTRL is reset after each loss of lock, typically once a day, and therefore is not sensitive to signals at frequencies lower than one inverse day, see Fig.(1).

5 Acknowledgments

I thank Daniel Sigg who designed and implemented the fsr readout channel, Bill Butler, Chad Forrest, Tobin Fricke and Stefanos Giampanis who were instrumental in the analysis of the data, and Valentin Rudenko for his interest and for useful discussions. I also thank Alan Kostelecky and Matt Mewes for the interpretation of the data in the “Standard Model Extension” framework, and for continuing advice.

The credit for the results discussed here belongs to the entire LIGO team.

6 APPENDIX

6.1 The free spectral range (fsr) of the arm cavities

The arms of the LIGO interferometers [13] consist of 4 km long, high finesse F-P cavities, that are kept on resonance in order to detect gravitational disturbances in the frequency range $40 < f < 8,000$ Hz. The light (carrier) frequency is of order $f_0 = \omega_0/2\pi \approx 3 \times 10^{14}$ Hz. The free spectral range of the cavities is $f_{fsr} = c/2L = 37.521$ kHz, and if sideband frequencies $f_{\pm 1} = f_0 \pm f_{fsr}$ circulate in the interferometer they *will resonate* in the arms. Such sideband frequencies will be modulated by mirror motion (in the arms) identically as the carrier. As pointed out by R. Weiss the circulation of an fsr sideband frequency represents a second interferometer that runs in the same optical system as the carrier. This “second” interferometer is privileged because it does not need to sense frequencies in the seismic region to keep the optics in lock. The optics are kept in lock by feedback based on the error signals derived from the main interferometer (the carrier). For the H1 LIGO interferometer, $f_{fsr} = 37.521$ kHz [14]. The transfer function from mirror motion, ω_s , to phase shift at the antisymmetric port, rises to unity at the fsr frequency just as it does at low frequencies for the carrier. Gravitational signals at the fsr frequency can be detected with maximal gain. But also low frequency gravitational signals can be detected with maximal gain, and are free of the low frequency noise, that dominates when the signal is extracted from the carrier.

Technically, this necessitates digitization of the signals at the antisymmetric port, ASQ and ASI, at higher frequencies $f_{adc} > 2f_{fsr}$. To record the signal at the fsr frequency the fast ASQ signal is demodulated by the RF frequency as usual. One copy of the fast ADC data was decimated and shifted by 37.504 kHz so as to be centered near the fsr frequency [15]. Such hardware was installed on the Hanford (H1 and H2) and Livingston (L1) interferometers for the S4 and S5 runs (2006-2007), with the principal aim to detect a stochastic background at the fsr frequency. No such high frequency background was detected and the upper limits were given in [16].

The *calibrated* (power density) spectrum for the H1 interferometer in the standard (low) frequency range, is shown in Fig.(8). It exhibits the well known rise (loss of sensitivity) at low frequencies due to seismic and other low frequency noise. The calibrated spectrum in the fsr region, covering the range $f = f_{fsr} \pm 1$ kHz, averaged over the entire run, was shown in Fig.(2). The sensitivity at the fsr frequency, which also corresponds to a signals near zero frequency is enhanced, and random noise is absent.

6.2 Detection of low frequency signals

When an fsr sideband circulates in the interferometer it is modulated by mirror motion, just as is the carrier. This leads to a detectable signal if only a *single* sideband circulates [17]. Serendipitously, such a sideband was present in the H1 interferometer because the large test masses (the mirrors of the arms) have a mechanical resonance near 37.890 kHz which is excited by the ambient thermal energy. The frequency of this mode is sufficiently close

to $f_{+1} - f_0 = f_{fsr}$, so that mirror motion, amplified by the light pressure, parametrically excites the f_{+1} field. The resonant mechanical motion of the test masses can not excite the lower sideband which is displaced by ~ 75 kHz (as compared to ~ 400 Hz for the upper sideband), thus satisfying the condition that only one sideband be present.

The amplitude of the sideband field can be extracted from the calibrated spectrum in the fsr region and is of order $E_{+1} \approx 10^{-7} E_0$, where E_0 is the carrier field. The low value of the (self excited) E_{+1} field explains why the calibration lines at ~ 50 and ~ 400 Hz are not seen in the spectrum of Fig.(2). In order to detect low frequency signals in the region of the fsr frequency a single fsr sideband, of adequate amplitude, must be *injected* into the interferometer.

An implication of the enhanced noise near zero frequency is the need for large “open loop” gain at low frequencies in order to keep the interferometer locked. This reduces the sensitivity of the interferometer response in that frequency region, since

$$h(f) = \frac{1 + G(f)}{C_0(f)} q(f), \quad (8)$$

where $q(f)$ is the signal at the AS-Q port, $C_0(f)$ is the optical sensing gain, and $G(f)$ the open loop gain. At low frequencies, where $G(f) \gg 1$, when an external strain $h(f)$ is imposed on the interferometer, the detected signal $q(f)$ is depressed and may become undetectable. This behavior is evident in Fig.(8) which shows the strain sensitivity of the H1 interferometer as measured by both the FSR channel, (H1 fast), and the conventional detection chain (H1 ASQ). Detecting low frequency signals at the fsr frequency *shifts* the detection to a frequency region where the feedback open loop gain is much lower, and thus the signal is significantly higher. Furthermore low frequency noise, but not that due to vibration of the optics, is absent.

Detection of signals at some frequency f_x represent external modulation of the phase shift between the two arms not only at f_x but also at $f = f_x - 37.504$ kHz because the spectrum has been shifted by that offset. Thus the power detected in a narrow region around 37.504 kHz is a measure of nearly static (DC) variations in phase shift.

Finally we note that the signal at the fsr frequency differs from the “canonical” recorded signals such as ASQ, DARM-ERR or DARM-CTRL in that it is not reset to zero when lock is reinstated. Thus it provides an *uninterrupted* record for signals with frequencies even lower than an inverse day, $f < 1.16 \times 10^{-5}$ Hz.

Having advocated for the detection of low frequency signals it is important to recall that at frequencies $f < 10$ Hz the interferometer becomes inoperable as a GW detector because the mirror suspensions have a natural frequency of order $\omega_s/2\pi \approx 10$ Hz, so that the mirrors can not be considered to be free test masses below that frequency.

6.3 Detection of very low frequency signals

Operating at the fsr frequency makes possible the detection of weak, very low frequency signals due to an unavoidable technical imperfection, namely a small *macroscopic* difference

in the length of the two arms, typically of order 1-2 cm. When the interferometer is locked the two arms are maintained at equal *microscopic* lengths, modulo λ_0 ,

$$L_x = m\lambda_0, \quad L_y = n\lambda_0 \quad m, n \text{ integers,}$$

where λ_0 is the carrier wavelength. However the macroscopic length of the two arms can differ by $\Delta L = L_x - L_y$; in that case the sideband frequencies $f_{\pm 1} = f_0 \pm (c/2L)$, which remain resonant in the arms, exhibit a phase shift⁵

$$\frac{\Delta\phi_{\pm}}{2\pi} = \frac{L_x - L_y}{\lambda_{\pm 1}} = \frac{L_x - L_y}{\lambda_0} \left(1 \pm \frac{c/f_0}{2L} \right) = \pm \frac{\Delta L}{2L}. \quad (9)$$

A residual macroscopic arm-length difference is always present and for the LIGO interferometers, it is of order $\Delta L \approx 2$ cm. This introduces at the fsr frequency a static ‘‘biasing’’ phase shift, which for a single traversal in the arms has the value

$$\Delta\phi^{(s)}/2\pi = 2.5 \times 10^{-6}.$$

The demodulated amplitude in the region of the fsr frequency is the sum of the amplitude A_{fsr} due to the biasing static phase shift, $\Delta\phi$, and the amplitude A_ω of any phase shift (signal) that may be imposed on the interferometer⁶. Thus the *power* in the fsr region

$$P = |A_{fsr} + A_\omega|^2 = |A_{fsr}|^2 + 2|A_{fsr}||A_\omega|\cos(\omega t + \phi) + |A_\omega|^2 \quad (10)$$

is modulated by the externally imposed (signal) amplitude A_ω . The modulation depth is a measure of the signal amplitude since A_{fsr} is fixed and can be directly inferred. The power at the fsr frequency is modulated to a depth M ,

$$M = \frac{P_{max} - P_{min}}{P_{max} + P_{min}} \quad \text{and if} \quad A_{fsr} \gg A_\omega \quad M \approx 2 \frac{A_\omega}{A_{fsr}}$$

The modulation M is the experimental observable, see Fig.(3), but to extract the phase shift $\Delta\phi_\omega$ at the dark port it is necessary to propagate the fields through the interferometer. Using the simulation code FINESSE [19] we find that modulation of 10% corresponds to a phase shift $\Delta\phi/2\pi = 10^{-10}$, in agreement with the expected phase shift from the horizontal component of the tidal gradients.

References

- [1] V.A. Kostelecky, A.C. Melissinos and M. Mewes, Phys. Lett. **B 761**, 1 (2016).
- [2] P. Melchior, *The Tides of the Planet Earth*, Pergamon Press, 1978.

⁵ This is analogous to the Schnupp asymmetry that allows the RF sidebands to reach the dark port while the carrier remains dark [18].

⁶ Equivalent to operating the interferometer off the dark fringe

- [3] S. Weinberg, *Gravitation and Cosmology*, John Wiley and Sons, NY, 1972.
- [4] J. B. Hartle, *Gravity: An introduction to Einsteins general relativity*, Addison Wesley, San Francisco, 2003.
- [5] Chad J. Forrest, “Tidal effects on Laser Interferometer Gravitational Detectors”, M.S. Thesis, University of Rochester (2008).
- [6] A. Melissinos (for the LSC), The effect of the Tides on the LIGO Interferometers, Twelfth Marcel Grossman Meeting on General Relativity, World Scientific, p.1718 (2012); arXiv:1001.0558.
- [7] J. D. Scargle, ApJ 263, 835 (1982); W. Press, W. Vetterling, S. Teukolsky and B. Flannery, Numerical Recipes in C++, Cambridge University Press, 1988.
- [8] A.A. Michelson and E.W. Morley, Am. J. Sci **34**, 333 (1887).
- [9] M. Nagel, et al., Nat. Commun. 6 (2015) 8174, arXiv:1412.6954v2 [hep-ph] 14 Sep 2015.
- [10] D. Colladay and V.A. Kostelecky, Phys. Rev. **D 55** 6760 (1997); D. Colladay and V.A. Kostelecky, Phys. Rev. **D 58**, 116002 (1998).
- [11] V.A. Kostelecky and N. Russel, arXiv:0801.0287
- [12] Eric Morganson, LIGO-T990181-00-WF.R.
- [13] A. Abramovici et al., Science **256**, 325 (1992).
- [14] W.E. Butler “Characterization of the High Frequency Response of Laser Interferometer Gravitational Wave Detectors”, Ph.D. Thesis, University of Rochester (2004).
- [15] D. Sigg, LIGO Document G040432-00-D (2004)
- [16] Stefanos Giampanis, “Search for a High Frequency Stochastic Background of Gravitational Waves”, Ph.D. Thesis, University of Rochester (2008).
- [17] A.V. Gusev, V.N. Rudenko and L.S. Yudin arXiv:1310.3104, see also A.C. Melissinos arXiv:1410.0854v2
- [18] L. Schnupp, Presentation at European Collaboration Meeting on Interferometric Detection of Gravitational Waves, Sorrento, 1988.
- [19] Andreas Freise, FINESSE, www.gwoptics.org/finesse.

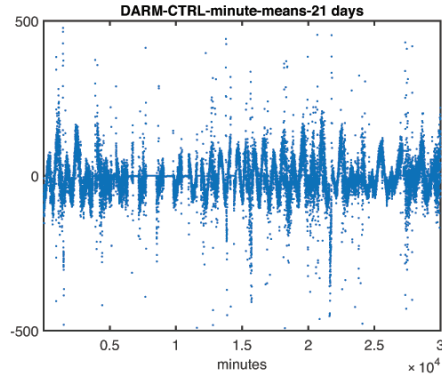


Figure 1: Minute trends of DARM-CTRL for 21 days

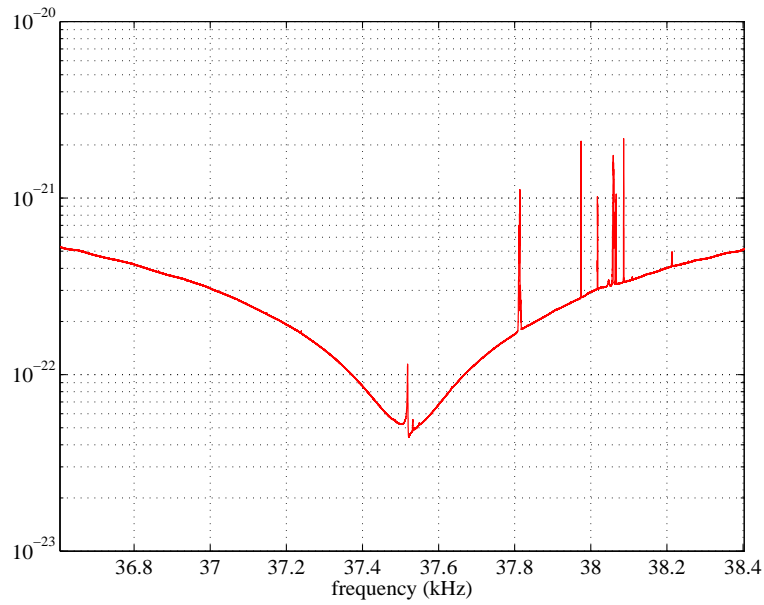


Figure 2: The strain sensitivity in the fsr region of the H1 LIGO interferometer in 2006, as measured by the FSR-1 channel. Modulation of the fsr signal in the DC region appears near $f = 37.504$ kHz, there is no seismic wall in that region. The discrete lines are due to the mechanical resonances of the test masses. This plot is an average over the entire run.

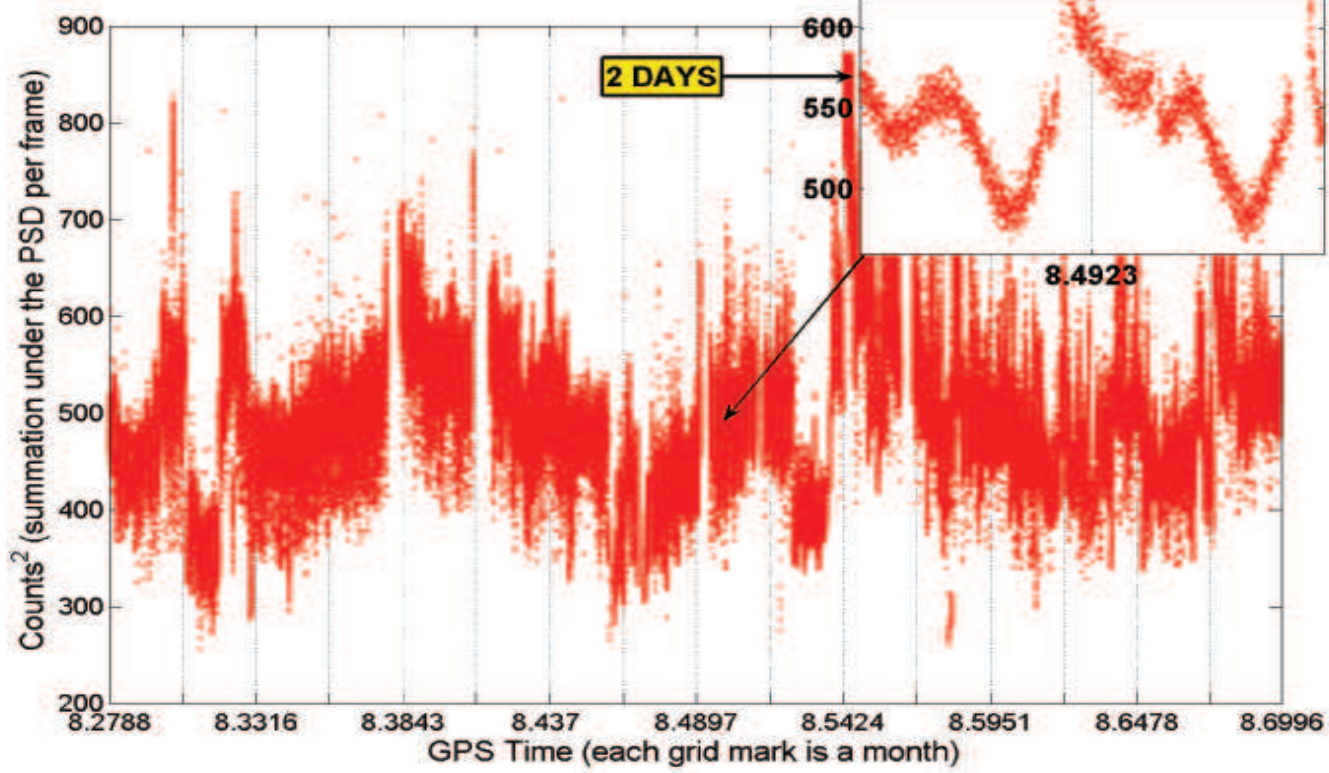


Figure 3: The integrated power spectral density in ± 200 Hz of the fsr as a function of time (at 64 second intervals) for 14 months during the S5 run. The daily and twice daily modulation can be seen in the inset. Vertical lines are at monthly intervals.

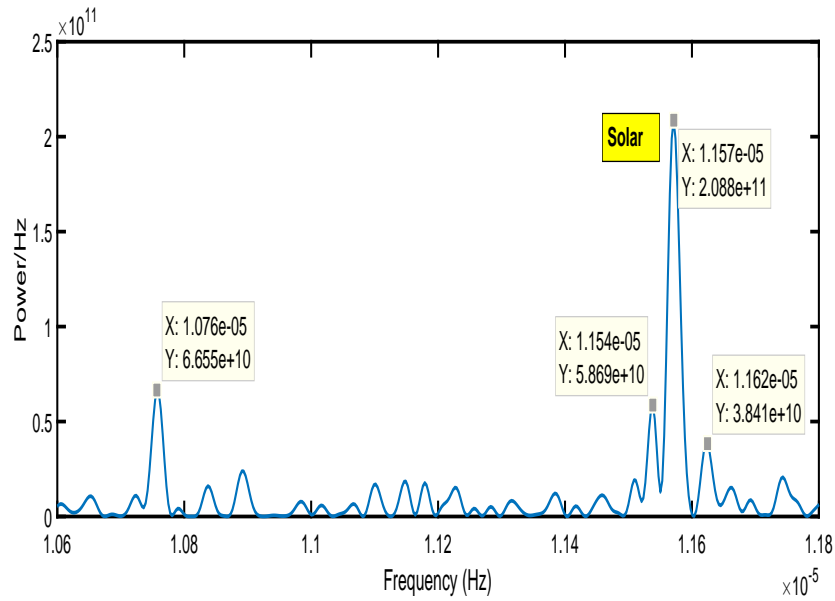


Figure 4: Power spectrum of the integrated power spectral density in the daily frequency region. Four tidal lines are clearly resolved.

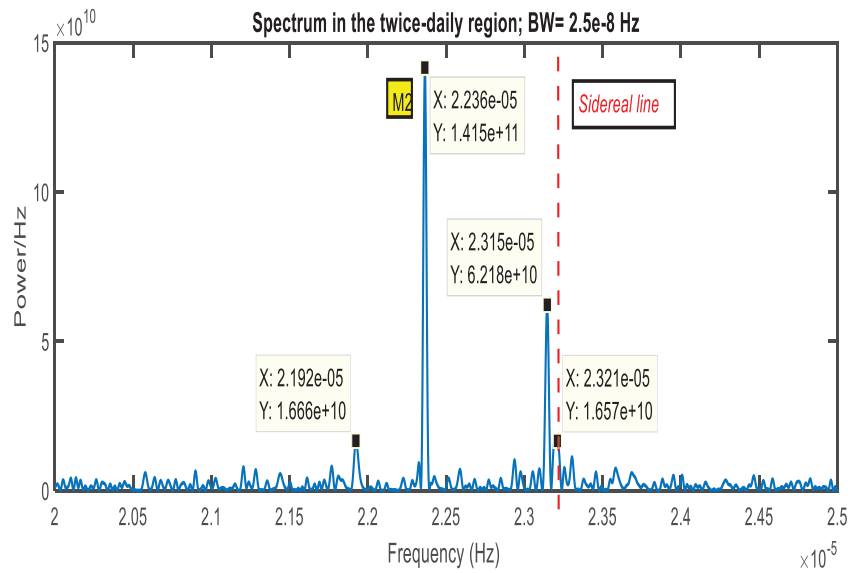


Figure 5: Power spectrum of the integrated power spectral density in the twice daily frequency region. Four tidal lines are clearly resolved and are labeled by their traditional symbols.

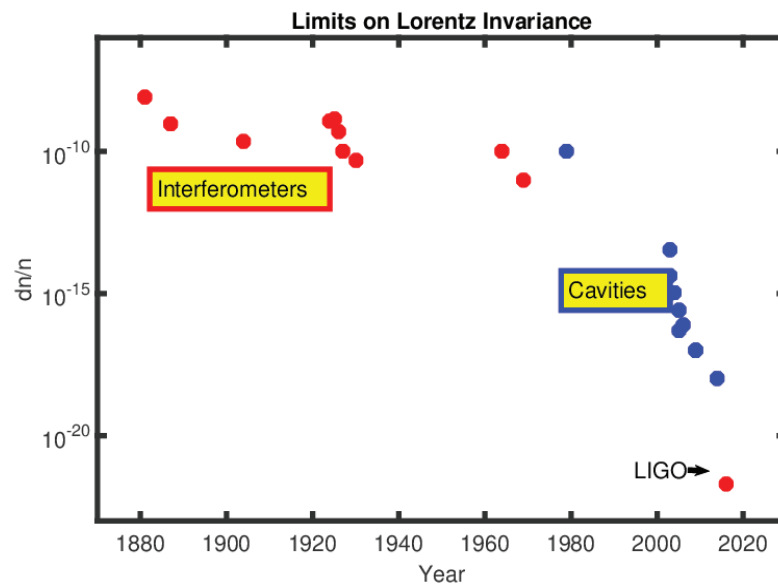


Figure 6: Limits on Lorentz Invariance violation in the photon sector over the past 140 years, from the absence of change in the effective refractive index of light as measured in the Earth's inertial frame. Points in red refer to interferometric measurements, while points in blue were obtained by rotating cavity experiments.

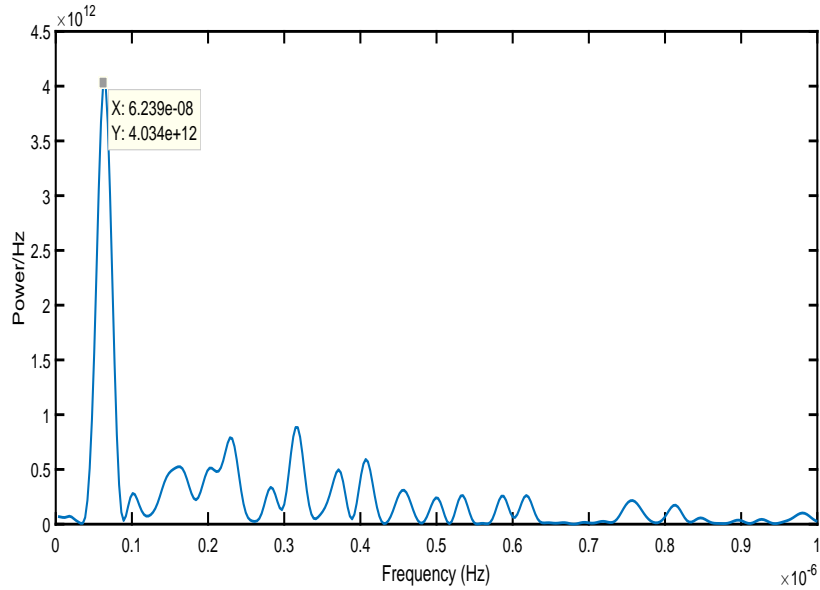


Figure 7: Power spectrum of the integrated power spectral density in the very low frequency region. The spectral line is at the twice yearly frequency within the measurement error.

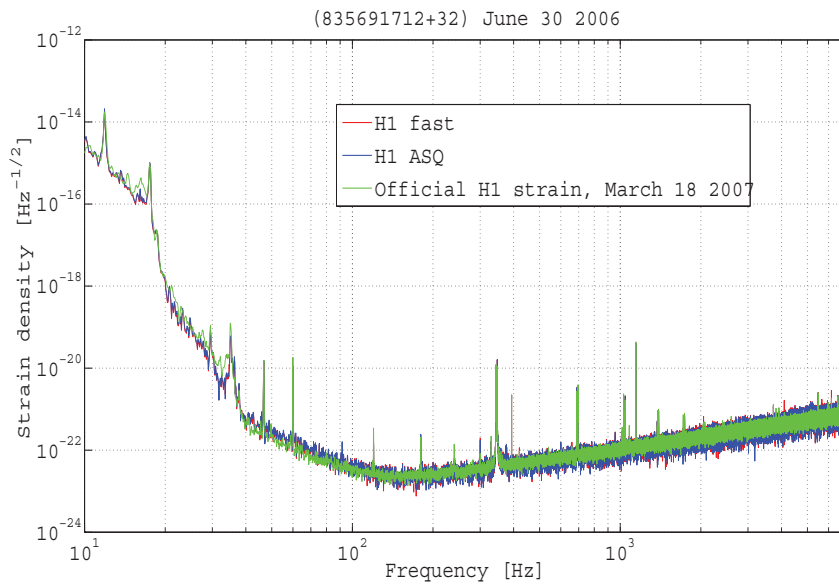


Figure 8: The (calibrated) sensitivity of the H1 LIGO interferometer in 2006, in the low frequency range as measured by the FSR channel (H1 fast) and by the conventional (H1 ASQ) channel. Below approximately 40 Hz rises the “seismic wall”. Compare to Fig.(2) in the region $f = 37.504$ kHz.